ELSEVIER

International Journal of Adhesion & Adhesives 22 (2002) 151–167

International Journal of Adhesion & Adhesives

www.elsevier.com/locate/ijadhadh

Mode I fracture of epoxy bonded composite joints 2. Fatigue loading

I.A. Ashcroft[a,*], S.J. Shaw[b]

[a] *Department of Mechanical Engineering, Wolfson School of Mechanical and Manufacturing Engineering, Loughborough University, Loughborough, Leicestershire LE11 3TU, UK*

[b] *Structural Materials Centre, Defence Evaluation and Research Agency, Farnborough, Hampshire GU14 0LX, UK*

Accepted 10 August 2001

Abstract

The main aims of this work were to investigate the effect of temperature on fatigue crack propagation (FCP) in bonded joints and to compare this with fracture under quasi-static loading and fatigue failure in uncracked lap joints. The fatigue tests were conducted on epoxy bonded carbon fibre reinforced polymer joints at −50°C, 22°C and 90°C and a number of techniques for determining strain energy release rate and crack propagation rate were evaluated. It was seen that temperature had a significant effect on the locus of failure and FCP, indicating that service temperature must be taken into account when designing bonded composite joints. The applicability of fracture mechanics data to the prediction of fatigue failure in uncracked lap joints was assessed by attempting to predict fatigue thresholds in two types of lap joints at three different temperatures. In most cases reasonable predictions were made, the notable exception being the overprediction of the fatigue threshold load in double lap joints tested at 90°C. This was attributed to creep in the double lap joints, which accelerated fatigue failure. It was recommended that in order to improve current prediction techniques, efforts should be made to base predictive methods on accurate physical models of the degradation and failure processes in the joints. © 2002 Published by Elsevier Science Ltd.

Keywords: A. Epoxides; B. Composites; C. Fracture mechanics; D. Fatigue; E. Environmental issues

1. Introduction

Fibre reinforced polymers (FRPs) are finding increased usage in a range of applications in the marine, automotive, sports and construction industries. However, it is perhaps the aerospace and defence sectors that have led the way for the utilisation of high specific strength and rigidity materials such as carbon fibre reinforced polymers (CFRPs). The weight savings to be gained by using high performance FRPs in aircraft can result in increased performance and payloads and this has resulted in their current widespread usage in fighter aircraft. Most structures are composed of constituent parts, which need to be joined together and the joint has the potential of being an area of structural weakness and/or of weight penalty. When joining FRPs, either to other FRP parts or to metal components, the most common techniques are mechanical joining (bolting or riveting) and adhesive bonding (including co-bonding and secondary bonding). Adhesive bonding is often the most structurally efficient technique and does not have the weight penalty of bolting and riveting. The necessity of drilling a hole in the composite for bolting and riveting may compromise the structural integrity of the FRP and results in a surface discontinuity which may need dressing. Adhesive bonding also results in a more even stress distribution which results in better fatigue performance and is very effective for joining dissimilar materials and thin sheet material. Of course there are also potential drawbacks in the use of adhesive bonding. These include a sensitivity to peel stress, which may limit the joining of thick sections, limitations in current NDE techniques for manufacturing quality assurance and in-service monitoring and difficulties in disassembly for inspection and replacement of parts. It is also recognised that adhesives can be environmentally sensitive and there is concern about the ability of adhesive joints to withstand the demanding environmental and loading

*Corresponding author. Tel.: +44-0-1509-223229; fax: +44-0-1509-223934.

E-mail address: I.A.Ashcroft@lboro.ac.uk (I.A. Ashcroft).

0143-7496/02/$ - see front matter © 2002 Published by Elsevier Science Ltd.
PII: S0143-7496(01)00050-1

conditions in structural applications in an aircraft. There is also uncertainty in the prediction of failure in bonded joints and a lack of validated design tools. There is, therefore, a need for a greater understanding of the fatigue performance of such bonded structures and, in particular, any degradation of that performance due to adverse environments, in order for the benefits of adhesive bonding to be fully achieved.

In Part 1 of this paper [1] the effect of temperature, within the range seen by a typical aircraft structure, on the quasi-static fracture of adhesively bonded, carbon fibre reinforced polymer (CFRP) joints was discussed. However, in almost all structural components, and obviously so in the case of aerospace structures, cyclical loads are encountered. It has already been shown in previous work that cyclically loaded adhesive joints can fail at a small percentage of the quasi-static strength (e.g. 26–62% in Ref. [2]). Cyclical fatigue loading must be considered, therefore, when designing bonded joints for aerospace applications. Two approaches have been used extensively in the characterisation of fatigue in bonded joints. These are the stress-life and fatigue crack propagation (FCP) approaches.

In the stress-life approach, a series of samples are tested at different fatigue loads, usually under constant amplitude fatigue loading. A plot is then made of stress (S) against the number of cycles to failure (N). A typical $S-N$ curve is shown in Fig. 1. In this case, a fatigue threshold is indicated, which is a load below which the part has an infinite fatigue life. When presenting fatigue data for bonded joints in this way there is the issue of what stress value to use. In many cases, when fatigue testing lap joints, the average shear stress amplitude has been used, which is obtained by dividing the load amplitude by the overlap area. However, in a bonded lap joint the shear stress is not uniform, there is no direct relationship between the average and maximum shear stresses and it is widely accepted that initial failure is attributable to the peel stresses rather than the shear stresses. It may appear preferable, therefore, to use the maximum peel stress. However, there is no simple way to calculate this analytically for lap joints and in finite element analysis some method of dealing with the singularity at the embedded corner of the adherend in the adhesive must be used to avoid a mesh-dependent maximum stress. The simplest solution is probably to present this data as an $L-N$ curve, plotting the maximum load (L) or load amplitude (ΔL) against N. It is obvious then that the results are only directly applicable to joints of the same type and the analysis that is required to apply the data to a different joint type can be dealt with separately. The effect of varying the mean stress (σ_m) and stress amplitude (σ_a) on the fatigue life can be shown on a Haigh diagram. This is a plot of σ_{m} against σ_{a} for constant life. A number of empirical relationships have been suggested to enable the effect of varying σ_{m} and σ_{a} to be predicted [3]. The stress-life approach is usually recommended for high cycle fatigue. For low cycle fatigue, a strain-life approach is preferred as this enables material plasticity to be accounted for [3].

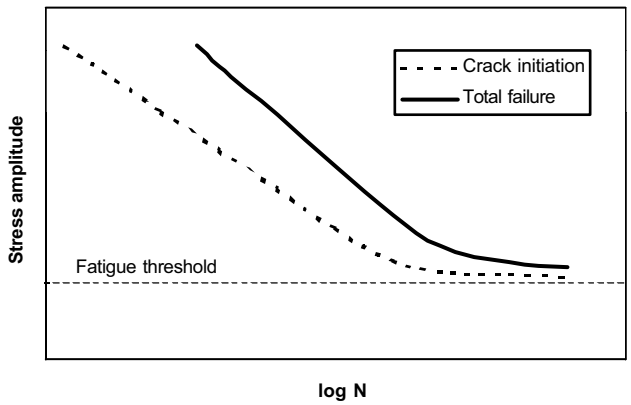

Fig. 1. Schematic $S-N$ curve.

Another feature of the $S-N$ approach is that usually only the number of cycles to complete failure is recorded. It is, therefore, not known what percentage of the total fatigue life is spent in initiation and propagation and this has been a source of disagreement within the scientific community. In all probability, this proportion is dependent on a number of factors including sample geometry, sample materials, presence of defects and voids and the applied load. There is also the difficulty in defining the transition from initiation to propagation, which in practice depends on the crack measurement technique that is used. Zhang et al. [4] used a back face strain technique to monitor fatigue propagation in single lap joints. They found that in the high load/low cycle range the fatigue life was dominated by propagation whereas in the low load/high cycle range the fatigue life was dominated by crack initiation. This is in agreement with the trend seen in the fatigue of metallic materials [3].

The authors have previously published work on the effect of temperature on the fatigue of double lap joints using the same materials as in the present study [2]. It was found that temperature affected the mechanisms and loci of failure as well as the magnitude of the loads required for fatigue failure. Complex failure paths were observed, with a tendency as temperature increased for the fracture path to change from failure in the composite adherends to cohesive failure in the adhesive bondline. Similar fatigue threshold loads were observed at 22°C and −50°C but a significant reduction in the fatigue threshold load was seen at 90°C. This was attributed to the deleterious effect of creep at elevated temperature. Chen et al. [5] also reported a significant decrease in the fatigue life of plastic–plastic and metal–plastic single lap joints when the test temperature was increased from 45°C to 55°C. Harris and Fay [6] tested single lap joints

with steel adherends in fatigue between −30°C and 90°C. They found that fatigue resistance decreased rapidly as the glass transition temperature (T_g) was approached and that there was a reduction in the dynamic stiffness of the joints during the fatigue tests, which they attributed to creep. They noted that at loads below the fatigue threshold there was no discernible creep and proposed that the fatigue life was dominated by the initiation phase.

The other main method of presenting fatigue data for bonded joints is aimed at measuring the rate at which the fatigue cracks propagate ($\mathrm{d}a/\mathrm{d}N$) and relating this to some fracture mechanics parameter such as the strain energy release rate (G), the stress intensity factor (K) or the J-integral. In these tests, the sample is usually pre-cracked and only the propagation phase is studied. This approach has been used extensively to characterise fatigue in metals, where $\log \Delta K$ is plotted against $\log \mathrm{d}a/\mathrm{d}N$ [3], and has also been applied to polymeric materials [7]. In the case of bonded joints, G is usually the most readily accessible fracture parameter and has hence been used by many researchers [8–13]. The results are usually presented as a logarithmic plot of $\mathrm{d}a/\mathrm{d}N$ against G. In testing adhesives and composites, the maximum strain energy release rate, G_{max}, is often used in preference to the strain energy release rate amplitude ($\Delta G = G_{max} - G_{min}$). This is because with polymeric materials, facial interference on unloading artificially raises G_{min} and therefore reduces the ΔG value. Mall et al. [14] tested double cantilever beam (DCB) and cracked lap shear (CLS) joints at different values of R (minimum load /maximum load) and showed in plots of G_{max} against $\mathrm{d}a/\mathrm{d}N$ that an improvement in fatigue performance was found at higher values of R. However, the data at different values of R could be reduced to a single curve when ΔG was plotted against $\mathrm{d}a/\mathrm{d}N$. Conversely, Knox et al. [15] showed a marked R-ratio effect in their plots of ΔK against $\mathrm{d}a/\mathrm{d}N$, which disappeared when they plotted G_{max} against $\mathrm{d}a/\mathrm{d}N$.

Plots of $\log G_{max}$ (or $\log \Delta G$) against $\log \mathrm{d}a/\mathrm{d}N$ yield a sigmoidal curve, as shown schematically in Fig. 2. Region I of the curve is associated with a fatigue threshold (G_{th}), below which measurable crack growth does not occur. G_{th} is an important parameter when designing with materials in which fatigue crack growth is to be avoided. In adhesives and composites, the crack propagation rate is generally more sensitive to changes in load than for metals and considerable scatter is often seen in the experimental FCP plots. This means that it is often desirable to base designs on fatigue thresholds with these materials. The fatigue threshold has been shown to be dependent on the loading configuration and environmental effects and has been the subject of considerable interest in the characterisation of fatigue in metals [16]. In region II the FCP curve is essentially

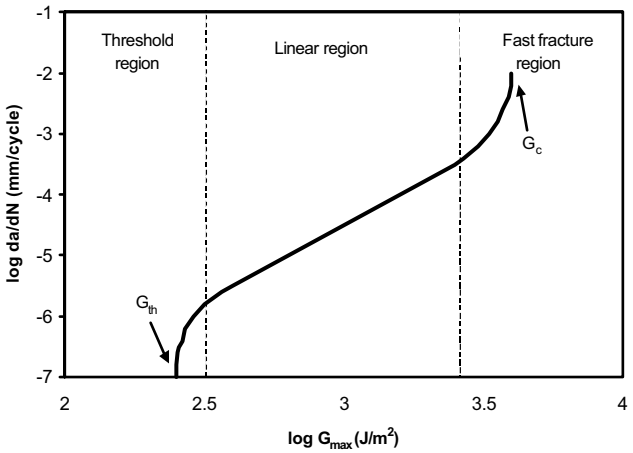

Fig. 2. Schematic fatigue crack propagation curve.

linear and in many cases the Paris relationship, given in Eq. (1), fits the data well.

$$\frac{\mathrm{d}a}{\mathrm{d}N} = C(G_{max})^m, \tag{1}$$

where C and m are material constants. The value of the exponent, m, indicates the load sensitivity of the crack propagation rate and is usually between 3 and 4 for metals but tends to be higher for adhesives [17,18] and FRPs [19,20]. Note that G_{max} can be substituted by a number of other fracture parameters in Eq. (3), including ΔG, ΔK and ΔJ. The most suitable fracture parameter will be dependent on the materials, geometry and loading conditions. In some structures, the fatigue life is dominated by crack growth in region II. In this case, Eq. (1) can be rearranged to predict the cycles to failure

$$N_f = \int_{a_i}^{a_f} \frac{\mathrm{d}a}{C(G_{max})^m}, \tag{2}$$

where a_i is the initial crack length and a_f is the final crack length.

Region III of the FCP curve signifies unstable crack growth as G_{max} approaches the critical strain energy release rate in quasi-static loading, G_c. The ratio G_{th}/G_c indicates fatigue sensitivity. In many applications, region III does not significantly affect the total propagation life and can be ignored in the prediction of cycles to failure. The full sigmoidal shape of the curve, however, can be described empirically by Eq. (3) [21]

$$\frac{\mathrm{d}a}{\mathrm{d}N} = C(G_{max})^m \left\{ \frac{1-(G_{th}/G_{max})^{m_1}}{1-(G_{max}/G_c)^{m_2}} \right\}, \tag{3}$$

where m_1 and m_2 are additional material constants. This can be rearranged to predict the total cycles to failure in the same manner that Eq. (2) was derived.

The DCB is probably the most popular type of joint for characterising FCP in bonded joints [22–25]. This

type of specimen consists of two cantilever arms, of uniform width and thickness, bonded together with a starter crack at one end. The load is applied perpendicularly to the loading arm, resulting in nominally pure mode I (opening mode) loading. It is a useful joint for studying crack propagation as the samples are relatively simple to manufacture and analysis methods are well established. There are many analytical methods available for the DCB and a number of these are discussed in Section 3.

Although the DCB has been widely used to investigate fatigue crack propagation in bonded joints, relatively little work has been published on the effect of temperature. Mostovoy and Ripling [26] found that when the test temperature for joints with a nitrile–phenolic adhesive was increased from room temperature to 56°C, the fatigue curve was shifted vertically upwards, indicating a higher crack propagation rate for a given ΔG, and there was a drastic reduction in G_{th}. They also noticed a change in the locus of failure as temperature increased, shifting from the adhesive to the primer/adhesive interface.

Kinloch and co-workers [27–29] have also used FCP curves from DCBs to predict $S-N$ curves in lap joints. Their methodology relies on two major assumptions. The first is that the fatigue life is dominated by propagation to a degree that means that the initiation phase can be ignored in predicting the total fatigue life. The second is that FCP data from a mode I test can be applied to a mixed mode failure. Both of these assumptions are the subject of some disagreement in the published literature and it would seem that further work is required to determine the limits of applicability of these assumptions.

In Part 1 of this paper [1], DCBs were tested at constant displacement rates at temperature of −50°C, 22°C and 90°C. Temperature was seen to affect the mode of failure, the locus of failure and the magnitude of the fracture energy. At low temperatures, brittle fracture was observed, with failure predominantly in the ply of the composite adjacent to the adhesive. At room temperature, stick–slip behaviour was observed, with mixed adhesive–composite failure in the slow crack growth region and failure predominantly in the composite in the fast fracture region. At high temperature, failure was predominantly by ductile failure of the adhesive. The quasi-static fracture energy increased with temperature. The results were explained with reference to a viscoelastic fracture model in which the critical strain energy release rate was dependent on the crack velocity. In this paper, the same joints are tested in constant amplitude fatigue over the same temperature range. The aim of the paper is to investigate the effect of temperature on the FCP curves and the locus of failure and to compare fatigue behaviour with the quasi-static fracture behaviour reported previously.

2. Experimental

2.1. Materials

The CFRP used in this study consisted of intermediate modulus graphite fibres in a modified bismaleimide/epoxy matrix. A unidirectional lay-up of 16 plies at 0° was used for the panels, which were autoclave cured at 182°C for 2 h, with an initial autoclave pressure of 0.6 MPa. The cured panels were scanned ultrasonically prior to bonding to check for defects. The samples were prepared in such a way that there were no detectable defects in the test gauge of the samples. The mechanical properties of the unidirectional laminates are given in Table 1. The panels were grit-blasted and degreased with acetone before bonding. The adhesive used was a proprietary modified epoxy, which was supplied as a nominally 0.2 mm film with a non-woven nylon carrier. The adhesive was based on a diglycidyl ether of bisphenol A epoxy, cross-linked with a primary amine curing agent. A reactive liquid polymer, based upon a carboxyl terminated butadiene acrylonitrile rubber, was used as a toughening agent. The formulation also contained a silica filler. Dumbell samples with a gauge length of 25 mm, gauge width of 4 mm and thickness of 3 mm were prepared from the film adhesive in order to determine the stress–strain behaviour of the adhesive at different temperatures and displacement rates. Results from samples tested at −50°C, 22°C and 90°C at a displacement rate of 1 mm/min are shown in Fig. 3.

2.2. Sample manufacture

In order to manufacture the DCB samples, panels of the cured CFRP were laid up with uncured adhesive film. A thin film (nominally 10 μm) of PTFE was placed at the bondline at one end of the panels to act as a starter crack. This assembly was auotoclave cured at 120°C for 60 min with a pressure of 0.6 MPa. After curing, a diamond saw was used to cut the samples to the dimensions shown in Fig. 4. The outer ends of the composite were then grit-blasted and degreased and brass hinges were bonded to the joint with a high peel strength adhesive that was cured overnight at 55°C. In order to enable accurate measurement of crack length

Table 1
Mechanical properties of CFRP

Property	Unidirectional laminate
E_1	174 GPa
E_2	9.64 GPa
G_{12}	7 GPa
ν_{12}	0.36
ν_{21}	0.02

the Krak Gage/Fractomat system supplied by RUMUL was used. The Krak Gages are thin strips of constantan, which are of constant thickness along the gauge length. These were bonded to the sides of the samples using a standard strain gauge adhesive. A constant current was applied to the gauge via the Fractomat. When a crack grows in the sample, the gauge tears, increasing the resistance of the gauge. This is measured by the Fractomat and converted to a crack length. More details of this system can be found in Refs. [30–32]. The output from the Fractomat was input to the computer data acquisition system via a strain channel on the test machine. A calibrated travelling microscope was used to check the calibration of the Krak Gages to an accuracy of 0.01 mm. The analogue nature of readings from the 'Krak Gage' give it an indefinite resolution and the manufacturers claim an accuracy of $>2\%$. This system, whilst costly and time consuming to set up, results in far better data than that obtained by the conventional method of optical measurement of crack length. However, care must be taken to ensure that the tearing of the gauge is a true reflection of the crack propagation in the sample.

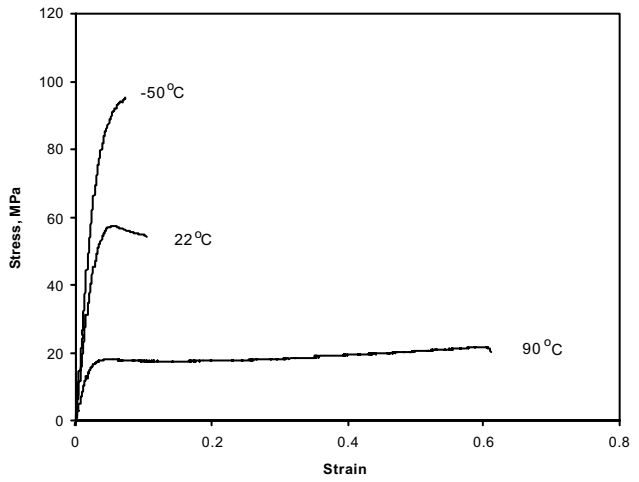

Fig. 3. Tensile stress–strain plots for the adhesive at different temperatures.

2.3. Fatigue testing

Crack growth is dependent on the control mode in constant amplitude fatigue tests. This is illustrated for the DCB in the current study in Fig. 5. It can be seen that in displacement control, G decreases with crack length whereas in load control G increases with crack length. If we assume that the crack growth rate is related to the strain energy release rate, as in Eq. (1), then this would predict that in load control crack growth is initially slow but accelerates until the sample has totally failed. Conversely, in displacement control we would predict rapid initial crack propagation that would decrease as the crack grows, potentially stopping before complete failure, if G_{th} is reached. This behaviour is useful as it allows us to generate the complete FCP curve from a single sample. In the current work, displacement control was used as this enables a number of tests at different displacements to be performed on a single sample and facilitates the determination of G_{th}. Results published in the literature indicate that whether a sample is tested in load or displacement control does not affect the relationship between strain energy release rate and FCG rate [14].

Testing was carried out using servohydraulic machines fitted with environmental chambers and computer control and data acquisition. The computer control was used to monitor crack length, load and displacement as a function of the number of fatigue cycles. Fatigue testing was conducted in displacement control, at a frequency of 5 Hz with a displacement ratio of 0.1. The crack growth rate decreased as the crack propagated and testing continued until a growth rate of <0.02 mm a day was recorded, which was used to define

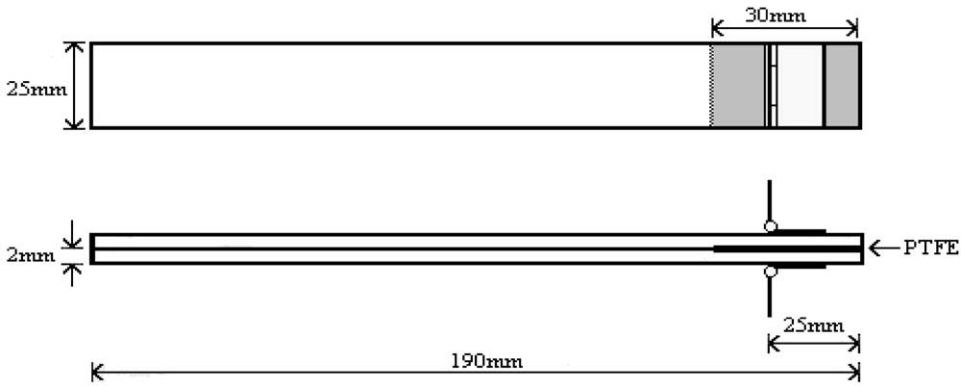

Fig. 4. Dimensions of double cantilever beam specimen.

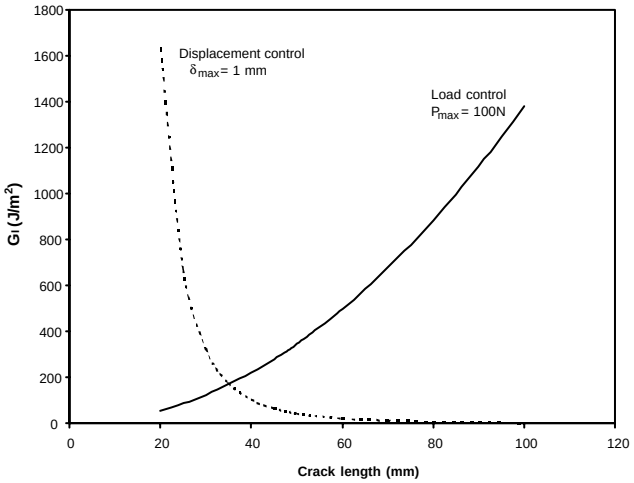

Fig. 5. Strain energy release rate as a function of crack length for a DCB in displacement and load control.

the fatigue threshold. At this point, the maximum displacement was doubled and another test started if sufficient gauge length remained. Due to crack growth arrest and a long usable gauge length, several fatigue tests could be run on a single specimen by increasing the maximum displacement used for each subsequent test run. Tests were conducted at -50°C, room temperature (22 ± 2), and 90°C. A minimum of three tests were performed at each temperature.

2.4. Fractography

The fracture surfaces were examined using both optical and scanning electron microscopy. Optical microscopy was used to study the locus of failure and to examine the appearance of the fracture surface. Samples for SEM analysis were then extracted using a diamond saw, and mounted on metal stubs. These were gold coated to ensure electrical conductivity.

3. Data reduction

Experimentally, we are measuring crack length, load and displacement as a function of cycles. The next step in the characterisation of FCP in the samples is to calculate the strain energy release rate and the crack propagation rate as a function of cycles from the experimental data. Various methods of performing these calculations are discussed below.

3.1. Calculation of G

The calculation of the strain energy release rate for a bonded DCB was discussed in some detail in Part 1 of this paper [1] and hence only a brief description of the methods used in the fatigue testing analysis are included in this paper. The energy criterion for crack growth [33] is based on the premise that a necessary condition for crack growth is that the stored elastic strain energy released when the crack grows must be at least as great as the energy required to create the new surfaces. When applied through a thickness crack in a plate of uniform thickness, b, and assuming linear elastic behaviour, the following equation can be derived for the strain energy release rate, G:

$$G = \frac{P^2}{2b}\frac{\mathrm{d}C}{\mathrm{d}a}, \tag{4}$$

where P is applied load, a is crack length and C is compliance (given by displacement divided by load). As load, displacement and crack length have been determined experimentally Eq. (4) can be used directly to calculate strain energy release rate as a function of cycles or crack length. A simple method of achieving this was explored by fitting a 3rd order polynomial curve to the full set of experimental compliance values plotted against crack length, giving an equation of the form:

$$C = Aa^3 + Ba^2 + Ca + D \quad \text{(Polynomial method)}, \tag{5}$$

where A, B, C and D are constants derived from the curve fitting exercise. The resulting equation was then differentiated and used to calculate $\mathrm{d}C/\mathrm{d}a$ as a function of a, enabling G to be calculated at all recorded crack lengths. A variant on this approach is the Berry method [34], which was also used in Part 1 of this paper. In this method, C is plotted against crack length, a, on a log–log chart. A straight line fit to this data gives a curve of the following form:

$$C = Ka^n, \tag{6}$$

where K is the intercept and n is the slope of the curve. Substitution of the above expression into Eq. (4) yields the following equation that can be used to calculate the strain energy release rate as a function of crack length:

$$G = \frac{nP\delta}{2ba} \quad \text{(Berry method)}. \tag{7}$$

If the elastic properties of the adherend material are known, then beam theory can be used to calculate the change in compliance of the DCB as a crack propagates. An expression for the compliance in a DCB, neglecting the contribution of the adhesive, is given by Eq. (8) [35]

$$C = \frac{2a^3}{3EI}, \tag{8}$$

where I, the second moment of area of the beam, is given by

$$I = \frac{bh^3}{12}. \tag{9}$$

Substitution of Eq. (8) into Eq. (4) yields the following expression for strain energy release rate as a function of crack length

$$G = \frac{12P^2a^2}{b^2h^3E} \quad \text{(CBT1)}. \tag{10}$$

It can be seen from Eq. (10) that when the elastic modulus of the adherend is known the displacement is not needed to calculate the strain energy release rate. In a similar way, an expression can be derived in which the strain energy release rate can be estimated from the elastic modulus and displacement when the load is not known [1]. The beam theory approach described above tends to underestimate the compliance as it is assumed that that the beams are built-in at the crack tip. A correction method that can be used to account for the deflection due to the beam-end rotation is to add a correction factor to the crack length [35,36]. This can be determined from an experimental plot of $C^{1/3}$ against a, where a residual crack length will exist at $C^{1/3} = 0$. The residual crack length is then simply added to the measured crack length.

A comparison of the three different methods of calculating the strain energy release rate for a DCB tested in fatigue at 22°C is shown in Fig. 6. It can be seen that the polynomial and Berry methods show excellent agreement at longer crack lengths but diverge at short crack lengths. The values computed using CBT1 tend to slightly overestimate G compared with the other two methods. This may be due to an error in the assumed value of elastic modulus or from the simplifying assumptions used in the derivation of Eq. (10). Similar trends are seen at other temperatures; however, the difference between the values calculated using CBT1 and those calculated from curve fitting to the experimental compliance data become more pronounced. This mirrors the trends shown in the calculation of G in the quasi-static tests and is discussed in more detail in Part 1 of the paper [1]. In the rest of this paper, the Berry method is used to calculate strain energy release rate as this provides a good fit to the experimental data in most cases and also allows a direct comparison with the quasi-static fracture energies calculated using this method.

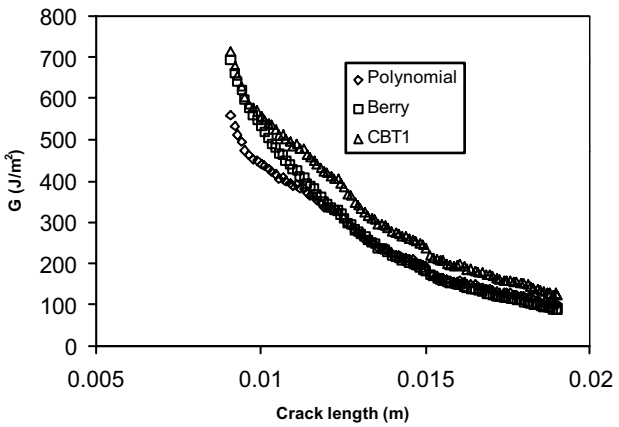

Fig. 6. Comparison of methods to calculate strain energy release rate as a function of crack length.

3.2. Calculation of $\mathrm{d}a/\mathrm{d}N$

A number of different approaches have also been used to calculate the crack growth rate from the experimentally determined crack length as a function of cycles. In this work, two different approaches were evaluated, both recommended in the standard test method for measurement of fatigue crack growth rates, ASTM E647-86a. The first was the secant method in which the crack propagation rate is calculated from the slope between adjacent points using Eq. (11)

$$\frac{\mathrm{d}a}{\mathrm{d}N} = \frac{a_{i+1} - a_i}{N_{i+1} - N_i}. \tag{11}$$

This is a simple method that accurately represents the data. However, the method is sensitive to scatter in the experimental data, which tends to be magnified in the calculation of $\mathrm{d}a/\mathrm{d}N$. The second method involves incrementally fitting a second order polynomial to sets of $(2n + 1)$ data points throughout the whole data set. The integer 'n' can be selected to ensure an appropriate number of data points for the curve fitting. The form of the polynomial equation for the incremental data fitting is

$$a = b_0 + b_1\left(\frac{N - C_1}{C_2}\right) + b_2\left(\frac{N - C_1}{C_2}\right)^2, \tag{12}$$

where b_0, b_1, and b_2 are regression parameters that are determined by applying the method of least squares to the data set. The terms C_1 and C_2 are used to scale the input data in order to avoid numerical difficulties in this process. $C_1 = 1/2(N_{i-n} + N_{i+n})$ and $C_2 = 1/2 \times (N_{i+n} - N_{i-n})$, where $i = (n + 1)$. The crack growth rate is then obtained by differentiating Eq. (12) with respect to N

$$\frac{\mathrm{d}a}{\mathrm{d}N} = \frac{b_1}{C_2} + 2b_2\left(\frac{N - C_1}{C_2^2}\right). \tag{13}$$

This method can reduce the scatter in the calculation of $\mathrm{d}a/\mathrm{d}N$, but there is a danger of masking real effects, especially if small data sets are used. A comparison of the secant and polynomial methods of calculating the crack propagation rate is shown in Fig. 7. For the polynomial method, the polynomial curve was fit to successive sets of 7 experimental data pairs (i.e. $n = 3$). It can be seen that there is good agreement between the two methods, although there is slightly more scatter with the secant method. In the rest of the paper, the polynomial method is used to calculate $\mathrm{d}a/\mathrm{d}N$ as this

reduces scatter and it is considered that the quantity of data obtained from the computerised data acquisition means that it is unlikely that any real effects will be masked.

An Excel macro was written using Visual Basic for Applications to aid analysis using the different approaches described above. By using the same method of calculating da/dN and G for all the samples, and using a numerical method of analysing the results, an objective comparison of the results can be made.

4. Results

4.1. Room temperature tests

Fig. 8 shows the variation in the maximum applied load (P_{max}) and crack length during a fatigue test at 22°C in displacement control. It can be seen that initial crack growth is rapid but slows until a constant crack length is reached. The plot of P_{max} against cycles appears to be an inverse of the plot of crack length against cycles, with an initial rapid decrease followed by a levelling to a constant value. This is to be expected, as a decrease in P_{max} is required to keep the maximum displacement constant as the compliance of the DCB increases with crack growth. These trends are as predicted from the calculated plot of strain energy release rate against crack length shown in Fig. 5. A similar increase in crack length and decrease in load was seen in the plots of load and crack length against time in the quasi-static tests [1]. This can be attributed to the increase in dC/da as the crack grows, which can be seen from Fig. 1 in Ref. [1] or by differentiating Eq. (7) with respect to a. From Eq. (4) it can be seen that the failure load would decrease as dC/da increases with constant fracture energy. It is noticeable that whereas the load and displacement data in quasi-static loading at room temperature showed that crack growth was not continuous but exhibited stick–slip behaviour, this is not evident in either the load or crack length traces for the same samples tested in fatigue. The time scale along the ordinate is far greater than that for the quasi-static tests. For example the 300 000 cycles in Fig. 8 correspond to 60 000 s, whereas quasi-static tests at room temperature were generally completed in <1000 s. However, even when the scale of Fig. 8 was enlarged to look for discontinuities in more detail no evidence of the stick–slip behaviour seen in the quasi-static tests was found.

The FCP plots for samples tested in fatigue at 22°C can be seen in Fig. 9. The results from 4 tests are shown and repeatability and scatter are reasonably good for

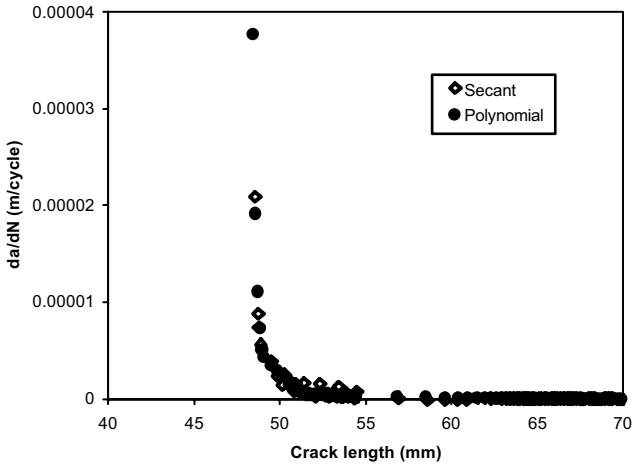

Fig. 7. Comparison of methods to calculate fatigue crack propagation rate as a function of crack length.

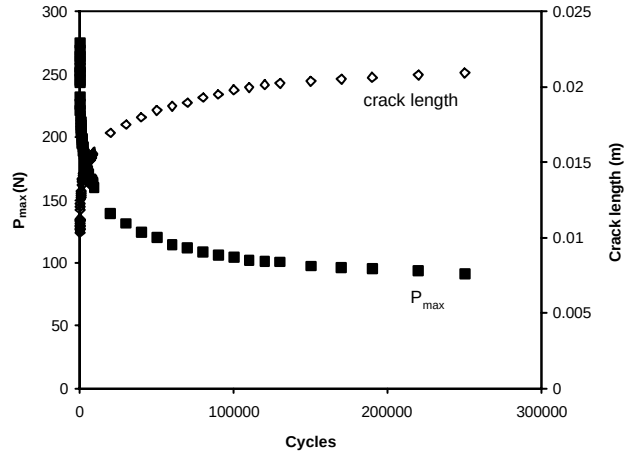

Fig. 8. Variation in maximum load and crack length during fatigue at 22°C.

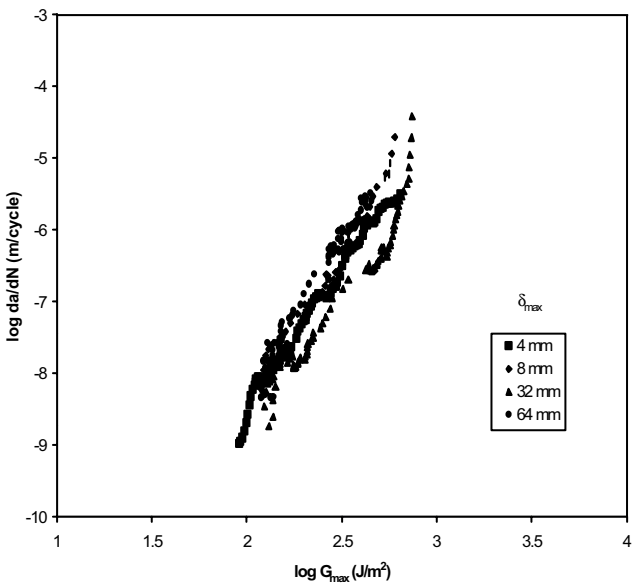

Fig. 9. Fatigue crack propagation curves at 22°C.

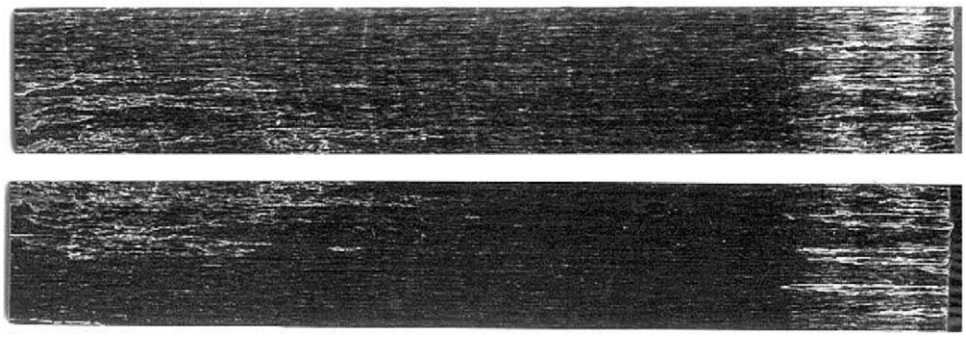

Fig. 10. Fracture surfaces of sample tested at 22°C.

this type of test and there is no obvious effect that maximum displacement has on the FCP curves. The curves exhibit an approximately sigmoidal shape, as discussed in Section 1. Region I is defined by the fatigue threshold with a mean strain energy release rate of 120 J/m^2. Region II shows a linear relationship between log G and log da/dN with a mean value for m of 3.4, which is similar to that seen in many metals. The fast crack growth in region II occurs at 400–500 J/m^2, which is comparable to the value of G_{Ic} for crack initiation in the quasi-static tests [1].

Fig. 10 shows the failure surface of a specimen tested in fatigue at 22°C. The specimen exhibits some striations, which were indicative of stick–slip behaviour in the quasi-static tests. These striations are not so marked as in the quasi-static tests but still indicate a change in the failure mode, with probably an accompanying discontinuity in the crack velocity. However, any such discontinuities must be on a far smaller scale than those seen in the quasi-static tests for them to be unobserved in the plots of load and crack length against cycles. Longitudinal strips near the starter crack (at the right side of the figure) show propagation in both adherends initially, with some cohesive failure of the adhesive. As the crack progresses, failure transfers predominantly to one of the adherends, with small regions of cohesive failure of the adhesive. Towards the end of the sample, a region similar to the initial fracture zone is observed. As in the quasi-static tests, the striations indicate areas of increased cohesive failure of the adhesive. Overall, there was a greater degree of cohesive failure of the adhesive than in the constant displacement rate tests at 22°C, but the dominant failure mode was still interlaminar failure of the composite.

4.2. High temperature tests

Fig. 11 shows the plots of P_{max} and crack length as a function of cycles for a fatigue test at 90°C. This shows the same trends as that seen in Fig. 8 for the fatigue tests at 22°C, i.e. P_{max} decreasing and a increasing with cycles until approximately constant values are reached. Logarithmic plots of G_{max} against da/dN for the fatigue tests at 90°C are shown in Fig. 12. There is no such pronounced knee in the curves in region I as seen at room temperature. The threshold strain energy release

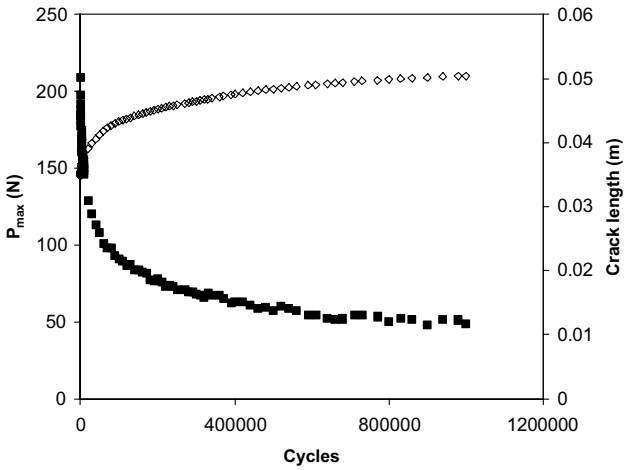

Fig. 11. Variation in maximum load and crack length during fatigue at 90°C.

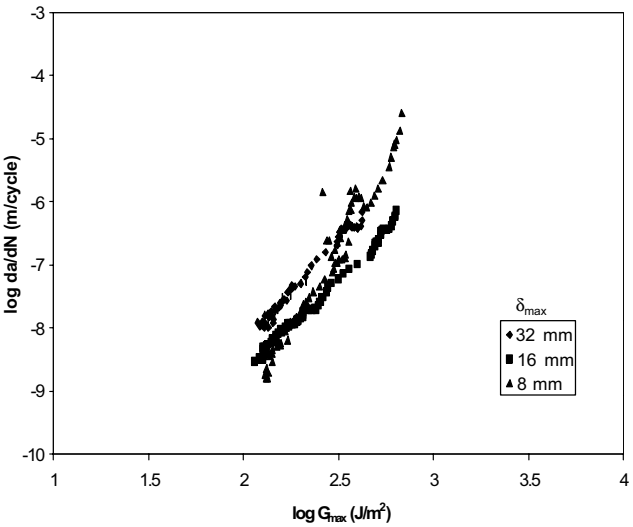

Fig. 12. Fatigue crack propagation curves at 90°C.

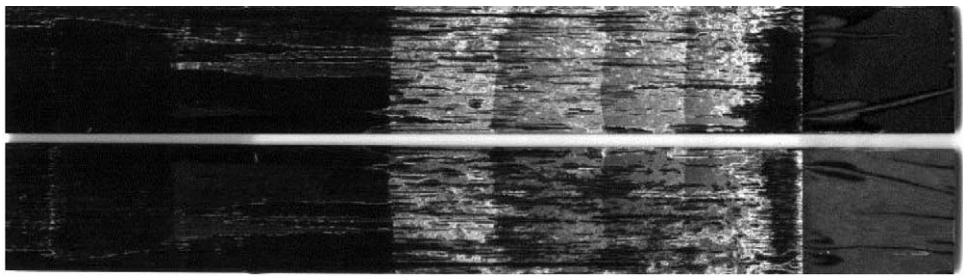

Fig. 13. Fracture surfaces of sample tested at 90°C.

rate is slightly higher than that seen at room temperature, with a mean value of 130 J/m^2. In region II, m is also slightly higher than that seen at room temperature with a mean value of 3.7. Region III is not so well defined for the high temperature fatigue tests as it was for the room temperature tests, however, there is an increase in the slope of the curve at about 700 J/m^2 for one of the tests. This is considerably lower than the value for G_{Ic} in the quasi-static tests, indicating that the fatigue tests have not fully characterised the fast fracture region in this case. This is not critical, as it is more important in fatigue predictions to establish G_{th} and the Paris equation constants in Region II. An example of a typical failure surface for a specimen tested in fatigue at 90°C can be seen in Fig. 13. The dominant failure mode was cohesive failure of the adhesive, the darker bands running parallel to the crack direction also indicate some composite failure. The transverse steps in the adhesive indicate where the crack stopped and the maximum displacement was increased to commence a new test; however, the transverse striations seen at the room temperature testing are not observed in the sample tested at 90°C. The dark region at the left side of the sample is the fracture surface created when the DCB was pulled apart at a high constant displacement rate in order to expose the fracture surfaces.

4.3. Low temperature tests

Plots of crack length and P_{max} against cycles for a fatigue test at −50°C are shown in Fig. 14. These plots take the same form as those shown in Figs. 8 and 11 for the fatigue tests at 22°C and 90°C. Some small discontinuities can be seen in P_{max} and crack length, e.g. around 550 000 cycles. However, these could not be positively identified with any feature in the fracture surface of the samples and it is impossible to state whether they are indicative of discontinuities in the crack growth or merely scatter in the experimental data. The FCP plots for the fatigue tests conducted at −50°C are shown in Fig. 15. Although there is a marked knee in the plots indicating a fatigue threshold, there is some variance in the location of the threshold. The mean value of G_{th} at this temperature is 80 J/m^2, which is lower than that seen at the higher temperatures. In region II, the gradient of the curve appears greater than that at the higher temperatures and this is reflected in a mean value for m of 8.8. Region III is not particularly distinct in the curves but occurs around 250 J/m^2, which is coincident with G_{Ic} from the quasi-static tests at −50°C.

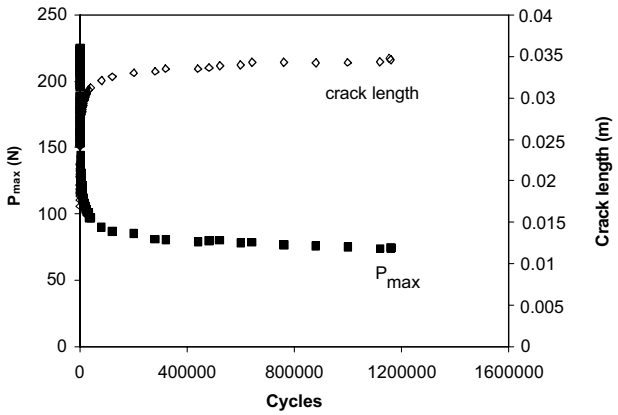

Fig. 14. Variation in maximum load and crack length during fatigue at −50°C.

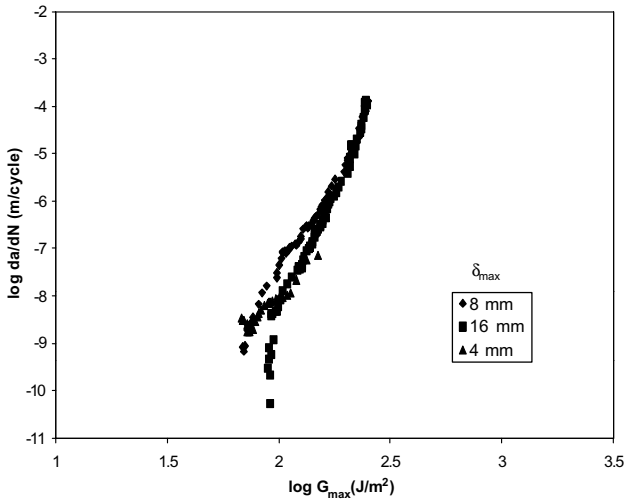

Fig. 15. Fatigue crack propagation curves at −50°C.

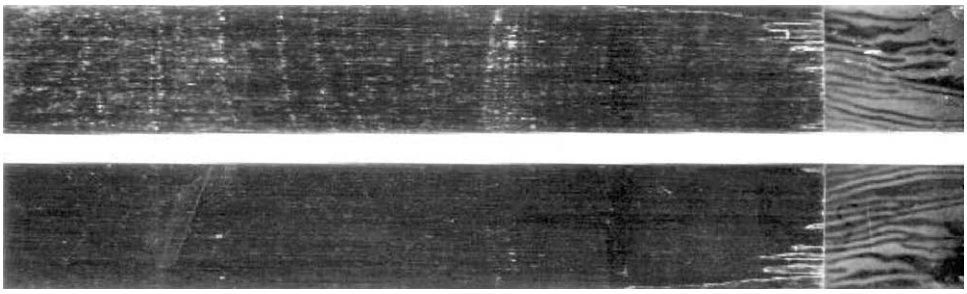

Fig. 16. Fracture surfaces of sample tested at −50°C.

Fig. 16 shows the fracture surface of a specimen tested in fatigue at −50°C. The starter crack is visible at the right-hand end of the specimen, with crack growth running from right to left. The dominant failure mode is fracture in the composite adherends. At the end of the starter crack, there are several white edged strips aligned with the direction of growth. These strips are regions where failure has begun in the top adherend, before passing through the adhesive into the lower adherend. The white edges are where the failure has passed through the adhesive layer and are therefore regions of cohesive failure in the adhesive. The specimen shown in Fig. 16 had been tested to zero growth 3 times, and the maximum displacement each time was doubled to facilitate further growth. The final phase of fatigue damage growth ended about 50 mm along the crack gauge. The specimen was then pulled apart to examine the failure surface. The dominant failure mode is in the top ply of the composite adherend, however, there are also small regions of cohesive failure of the adhesive, though less than that in the sample tested at room temperature. There are also faint striations on the fracture surface where there is an increased percentage of cohesive failure of the adhesive. However, as with the room temperature tests these cannot be assigned to any noticeable discontinuities in the plots of P_{max} and crack length against cycles.

5. Discussion

5.1. Analysis methods

In most of the fatigue tests analysed, the Berry method and the polynomial curve fitting approach to the calculation of strain energy release rate showed good correlation with one another. Mostovoy et al. [36] derived the following expression for the compliance of a DCB as a function of crack length:

$$C = \frac{8a}{bEh^3}(a^2 + h^2). \tag{14}$$

It can be seen that a 3rd order polynomial, as given in Eq. (5), is capable of fitting a plot of C against a of this form, the constants B and D being zero. If $a \gg h$, Eq. (14) simplifies to Eq. (8) (i.e. the expression for the compliance used in deriving the CBT1 expression for G). In this case, Eq. (6) (i.e. the expression for compliance used in deriving the Berry expression for G) can be used to fit a plot of C against a; the exponent term, n, being 3. It can be seen, therefore, that both the Berry method and 3rd order polynomial methods are reasonable approaches for deriving the strain energy release rate from the experimental compliance and this is confirmed by the good agreement between the two methods. In curve fitting to the experimental data it was seen that n in Eq. (6) was not exactly 3 and constants B and D in Eq. (5) were not exactly zero. This is probably inevitable given the unavoidable existence of experimental scatter, however, this may also be a way that these expressions are capable of fitting the experimental data well when the assumptions used in determining Eqs. (8) and (14) are not strictly valid. It is interesting to note in Fig. 6 that the agreement between the two curve fitting methods is poorer at small crack length, where the condition $a \gg h$ is less applicable. It should be noted, however, that in displacement control the short crack effects are only significant in the initial stages of crack growth where G and da/dN are high, whereas the main interest in this work is in determining fatigue thresholds. Moreover, if this effect was significant in the current tests then a repeatable difference between the FCP curves in region III would be expected at different displacements, whereas it can be seen from Figs. 9, 12 and 15 that this is not the case.

The beam theory method (CBT1) of calculating G showed reasonable agreement with the experimental compliance methods at 22°C, but was less successful at other temperatures. The two main drawbacks in using this method are the reliance on an accurate knowledge of the elastic modulus of the adherends and the simplifying assumptions used in deriving the expressions for G. Attempts to address the latter have been made by deriving expressions for G which take into account the adhesive layer [37,38] and large scale deflection [39] and

by using FEA [12]. However, these methods tend to be more complex to apply and some simplifying assumptions and the reliance on material data remains. This material data is not always easy to obtain and may be time- and environment-dependent as well as subject to batch variability. It is, therefore, recommended that when experimental compliance data has been obtained that this should be used in the calculation of G. In this paper, the Berry method was chosen in preference to the polynomial method for consistence with Part 1 of the paper.

Of the two different methods used for calculating da/dN, both the seven-point polynomial curve fitting approach and the secant method showed the same trends. However, the polynomial method showed less scatter in the results than using the secant method, and so this was used in conjunction with the Berry method to plot da/dN against G.

5.2. Effect of temperature

Table 2 shows a summary of the fatigue results at different temperatures. The threshold value of strain energy release rate, G_{Ith}, increases with temperature, although the differences are not as significant as those seen in the quasi-static testing. This may be due to the different fracture mechanisms involved in fatigue and constant displacement testing or to the difference in the crack propagation rates in determining G_{Ic} and G_{th}. It was demonstrated in Part 1 of this paper [1] that stick–slip behaviour was dependent on the displacement rate and this will vary in a sinusoidal waveform. The fatigue threshold values are in good agreement with those in the literature, which report G_{Ith} for interlaminar failure of the composite [40] at 50–100 J/m^2, and around 200 J/m^2 for cohesive failure of the adhesive at room temperature [29]. The results from the bonded composite are higher than the quoted values for the composite and lower than that for the adhesive. This is reasonable as the fracture surface in the bonded composite joints exhibited both adhesive and composite failure. The ratio G_{Ith}/G_{Ic} as a function of temperature is also shown in Table 2. This ratio indicates how sensitive the sample is to fatigue loading. A high value indicates that the fatigue threshold load is close to the quasi-static failure load and that special consideration of fatigue does not need to be taken into account during design. A low value means that the samples will fail in fatigue at a small fraction of the failure load in constant displacement rate loading, and that fatigue needs to be taken specifically into account if fatigue loads are expected in-service. It can be seen in Table 2 that as temperature increases so does the importance of fatigue in design consideration of the joint.

In Table 2, m is the slope in the linear region of the logarithmic plot of G against da/dN (or the exponent in Eq. (1)). This parameter indicates how sensitive the crack growth rate is to changes in the fatigue load in the steady state region. A high value for m indicates that a small increase in the load will result in a large increase in the crack growth rate. Caution must be exercised in predicting fatigue propagation life for materials with high values of m as the crack growth rate and hence fatigue life will be extremely sensitive to fluctuations in the applied load. It can be seen in Table 2 that there is little difference in the value of m at 22°C and 90°C but that a large increase in m is seen at −50°C.

Table 2 also summarises the locus of failure. At −50°C failure is predominantly in the top ply of the composite adherend. At 22°C failure in the composite and the adhesive can be seen and at 90°C cohesive failure of the adhesive is the dominant failure mode. This trend is seen in samples tested quasi-statically and in fatigue. No significant differences were seen in the fracture surfaces tested in fatigue and quasi-statically. However, as the main aim of the fractographic examinations were to establish the locus of failure, differences in the micro-mechanisms of failure may be observed by more detailed studies. The fracture mechanisms in rubber toughened epoxies have been studied extensively [41–44] but relatively little work on the fatigue fracture mechanisms has been reported. However, a recent study [45] has indicated that there is a threshold K (or G) value below which the toughening

Table 2
Summary of DCB results

Temperature	G_{Ic} (J/m^2)	G_{Ith} (J/m^2)	m	G_{Ith}/G_{Ic}	Dominant failure mode
−50°C	250±50	80±10	8.8±0.9	0.32	C[c]
22°C	200±50[a]				C
	500±100[b]	120±12	3.4±0.5	0.24	C and A[d]
90°C	1500±500	130±5	3.7±0.9	0.09	A

[a] Crack arrest in stick–slip growth.
[b] Crack initiation in stick–slip growth.
[c] C = failure in composite.
[d] A = cohesive failure in adhesive.

mechanisms associated with rubber toughening, e.g. shear yielding and cavitation, are not activated. This was associated with the small plastic zones at low K. This work was performed on bulk polymer samples and it would be interesting in future work to see if similar arguments apply to bonded joints and to observe the effect of temperature on these fracture mechanisms.

5.3. Comparison with lap joints

It is interesting to compare the effect of temperature on the fatigue fracture of the DCBs with the effect of temperature on the fatigue behaviour of bonded lap joints. Double lap joints and lap-strap joints were manufactured with the same materials used in the present study and tested in fatigue at the same temperatures. The geometry of these samples are shown in Fig. 17 and more details of the manufacture and testing of the lap-strap and double lap joints can be found in Refs. [46,2], respectively. A summary of the results from these different tests can be seen in Table 3. Only the results from the double lap joints and lap-strap joints with unidirectional adherends are presented to enable the most direct comparison with the DCB results. For both lap-strap and double lap joints, the fatigue threshold load was defined as the highest maximum load that the samples could survive 10^6 cycles without exhibiting any damage as indicated by optical microscopy. In order to allow a direct comparison between the different joint types, the strain energy release rate at the threshold load was estimated for the lap-strap and double lap joints using continuum mechanics and finite element analysis. In the case of the lap-strap joint, the equation derived by Brussat et al. [47], based on simple beam theory, was used to estimate the total strain energy release rate. For a lap-strap joint with equal thickness adherends, this expression reduces

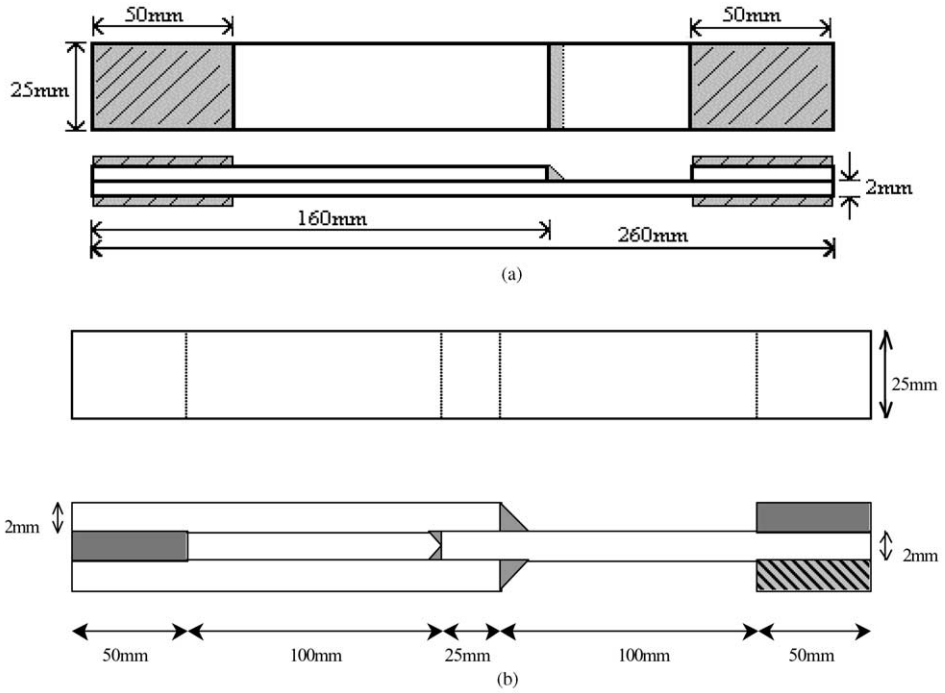

Fig. 17. Dimensions of (a) lap-strap and (b) double lap joints.

Table 3
Effect of temperature on the fatigue thresholds of different joint types

Temp. (°C)	Lap-strap joint			Double lap joint		
	P_{th} (kN)	G_{th} (BT) (J/m0^2)	G_{th} (FEA) (J/m^2)	P_{th} (kN)	G_{th} (BT) (J/m^2)	G_{th} (FEA) (J/m^2)
−50	14 (±1)	225	203	10.1 (±0.5)	78	106
22	15 (±1)	252	202	10.0 (±0.5)	77	105
90	14 (±1)	225	176	3.3 (±0.2)	8.3	12.3

to Eq. (15)

$$G_T = \frac{P^2}{4b^2Eh}. \quad (15)$$

In order to estimate the threshold strain energy release rate for the double lap joints the expression derived by Spelt et al. [48] using the J-integral, together with large deformation beam theory, was used. For the situation where the outer and inner adherends are of the same thickness, h, this expression reduces to Eq. (16)

$$G_T = \frac{P^2}{6b^2Eh}. \quad (16)$$

It should be noted here that Eqs. (15) and (16) have only been used to provide an estimate of the strain energy release rate in order to allow like quantities to be compared for all the joints tested. However, some confidence can be gained in using these equations as they have been shown to be in reasonable good agreement with finite element analysis [49]. It should be remembered though, that these equations are subject to the simplifying assumptions used in their derivation and the material properties used, as with Eq. (10) for the DCB. The reason that G_T is used for comparison rather than G_I (or some other parameter) is because G_T has been shown [50] to be the more appropriate failure parameter when comparing adhesively bonded DCB and lap-strap joints with composite adherends. The finite element estimations of strain energy release rates for double lap joint and cracked lap shear joint were based on plane strain models and the virtual crack closure method. More details of the finite element analyses can be found in Ref. [51] for the lap-strap joint and Ref. [52] for the double lap joint.

Comparing the results in Tables 2 and 3 it can be seen that the different joints respond quite differently to temperature. The fatigue threshold tends to increase with temperature for the DCBs, indicative of an increase in fracture toughness, whereas the lap-strap joint exhibits a slight decrease in fatigue threshold at high temperatures and the double lap joints exhibit a very large decrease in fatigue threshold at high temperatures. It can also be seen that there are marked differences in the values of G_{th} for the different joint types at all temperatures. This raises doubts about the applicability of DCB fracture data to the prediction of fatigue thresholds in lap joints. A number of factors may explain these differences including, the effect of mode mix on fatigue threshold, the assumptions made in the calculation of strain energy release rate and the mechanisms of fatigue failures in the different joint types.

If the strain energy release rate is to be used as the failure parameter, the calculation of this parameter with the different joints should be studied. The calculation of G for the DCB would have been thought to be fairly straightforward as the joint has a well-established crack and simple geometry. However, both parts of this paper have shown that errors in the calculation of G can arise when using beam theory methods and FEA prediction because of the simplifying assumption made in the analyses and the dependence on the values of material properties, which may demonstrate large batch variance. An experimental compliance method was, therefore, recommended for the calculation of G in DCB joints. The G_{th} in the DCBs is defined as the arrest of a well-established crack, subjected to nominally symmetrical, pure mode I loading. In the lap-strap joint, we defined the fatigue threshold as the highest fatigue load an uncracked joint could withstand 10^6 cycles. It is noted that pre-cracked lap-strap joints have been used to generate fatigue thresholds as defined by crack arrest, as with the DCB, however, in this investigation it was considered that the application to uncracked joints is a more realistic scenario. We, therefore, have quite different definitions of a fatigue threshold in the two types of joint. In the DCB, we have arrest of a propagating sharp crack and in the lap-strap joint we have initiation in an uncracked joint, accepting that there will exist flaws that may act as sites of failure initiation. In order to calculate the threshold strain energy release rate for the lap-strap joint, we must assume an initial flaw size and location. In the lap-strap joint, it has been shown that for well developed cracks the total strain energy release rate and mode mix are relatively constant with crack length for a given applied load [49]. It has also been shown that the calculated strain energy release rate is not very sensitive to the location of the crack [51]. We must look elsewhere then for the difference in the value of G_{th} between the DCB and lap-strap joints. In all the calculations to date, it has been assumed that the crack is through the fillet, however, an embedded flaw would result in a decrease in the strain energy release rate [53], which would reduce the value of G_{th} for the lap-strap joint. The shape and size of the assumed flaw may also be of importance. It has already been shown in Part 1 of this paper that a blunt crack requires a higher value of G to propagate than a sharp crack. It was also shown that crack arrest and crack propagation values can be quite different and this was attributed to the dependence of critical strain energy release rate on crack velocity. This may also have a similar, though perhaps less significant effect in fatigue crack initiation and propagation. Crack size may also be important, Pradhan et al. [53] have indicated that strain energy release rate tends to zero as crack size tends to zero and at very small crack lengths strain energy release rate will decrease. This is not always obvious in FE results because of mesh size and edge effects at very small crack lengths. Two other possible factors should also be mentioned. One is that

Table 4
Fatigue threshold predictions in lap joints

Temp. (°C)	Lap-strap joint			Double lap joint		
	Expt. (kN)	Predicted (kN)	Error (%)	Expt. (kN)	Predicted (kN)	Error (%)
−50	14	8	43	10	10	0
22	15	10	33	10	12.5	25
90	14	11	21	3.3	13	294

the lap-strap joint is a mixed mode test and although G_T has been proposed as a failure criterion applicable for different modes this is not necessarily correct in all cases. Finally, the threshold values in the cracked lap shear joints were calculated using the manufacturer's values for CFRP properties and adhesive properties from in-house tests, and possible errors from using these values have already been highlighted in this paper. With the double lap joint, most of the arguments listed for the lap-strap joint are relevant; however, we also have the additional factor that strain energy release rate and mode mix are dependent on crack size at all crack lengths [53].

In Table 4, the fatigue thresholds in the lap-strap and double lap joints have been predicted from the DCB fatigue threshold using the simple beam theory analyses. It can be seen that in all cases, except for the double lap joints at 90°C, the predictions are reasonable and probably as good as to be expected given the simplifying assumptions made in their derivation. There is still, however, the temptation to vary the method of calculating G, the failure parameter, the assumed crack size or the material properties to improve the predictions further. However, this may result in the right answer for the wrong reasons and clearly does little to commend the robustness of this prediction method. The reason for the lower predicted fatigue threshold for the double lap joint at elevated temperatures can be attributed to the effect of creep in this joint and this has been discussed in some detail in a previous paper [2].

In summary, the application of fracture mechanics data to the prediction of fatigue failure in uncracked lap-joints is capable of reasonable predictions but there are still a number of issues which need to be settled in order to create a robust predictive method that is not subject to arbitrarily chosen parameters in the analysis. Perhaps, the most pertinent question, however, is whether fracture propagation data should be used to predict fatigue thresholds when damage initiation must be the dominant concern in predicting fatigue thresholds in uncracked joints. Perhaps, a more mechanistically realistic alternative would be to use a damage mechanics approach to model the initiation process [52] followed by a viscoelastic fracture mechanics approach to model the propagation phase. It should be realised though that this science is not well developed and in the meantime a semi-empirical approach based on a more simplistic analysis is the only practical approach available to the designer. Efforts should thus be made to further validate these methods in order to determine their limits of applicability and to create simple but robust design methods.

6. Concluding remarks

The experimental investigation has shown that temperature, in the range seen in aerospace applications, has a significant effect on the fatigue crack propagation in bonded CFRP joints. As temperature increased, G_{th} increased, and the ratio G_{th}/G_{Ic} decreased. It was also seen that the locus of failure transferred from the composite adherend to the adhesive layer as temperature increased from −50°C to 90°C, as seen in the quasi-static tests. A number of methods of determining the strain energy release rate were investigated and, as with the quasi-static tests, it was recommended that experimental compliance methods should be used when experimental data is available.

The G_{th} values determined from the DCB tests were then used to predict fatigue thresholds in two types of lap joint. G_T at the 10^6 cycles fatigue threshold was used as the failure criterion and simple analytical methods were used to calculate G_T for the lap joints. Reasonable predictions were seen in all cases, except for the double lap joints tested at 90°C, in which case premature failure was attributed to the effects of creep. The effect of simplifying assumptions in the analysis have been discussed and it is felt that the most likely route to improving current predictive methodologies is by developing failure models more closely related to the degradation and failure mechanisms occurring in the joints.

Acknowledgements

The authors would like to acknowledge the contribution made by Darren Hughes to the experimental work described in this paper.

References

[1] Ashcroft IA, Hughes DJ, Shaw SJ. Mode I fracture of epoxy bonded composite joints: Part 1. Quasi-static loading. Int J Adhesion Adhesives 2001;21:87–99.

[2] Ashcroft IA, Hughes DJ, Shaw SJ, Abdel-Wahab M, Crocombe A. Effect of temperature in the quasi-static strength and fatigue resistance of bonded composite double lap joints. J Adhesion 2001;75:61–88.

[3] Bannantine JA, Comer JJ, Handrock JL. Fundamentals of metal fatigue analysis. Englewood Cliffs, NJ: Prentice Hall, 1990.

[4] Zhang Z, Shang JK, Lawrence FV. A backface strain technique for detecting fatigue crack initiation in adhesive joints. J Adhesion 1995;49:23–36.

[5] Chen NNS, Niem PIF, Lee RC. Fatigue behaviour of adhesive bonded joints. J Adhesion 1987;21:115–28.

[6] Harris JA, Fay PA. Fatigue life evaluation of structural adhesives for automotive applications. Int J Adhesion Adhesives 1992;12: 9–18.

[7] Hertzberg RW, Manson JA. Fatigue of engineering plastics. Academic Press: New York, 1980.

[8] Everett R, Johnson WS. Repeatability of mixed-mode adhesive debonding, ASTM STP 876. Philadelphia: American Society for Testing and Materials. p. 267–81.

[9] Jablonski DA. Fatigue crack growth in structural adhesives. J Adhesion 1980;11:125–43.

[10] Lin C, Liechti KM. Similarity concepts in the fatigue fracture of adhesively bonded joints. J Adhesion 1987;21:1–24.

[11] Luckyram J, Vardy AE. Fatigue performance of two structural adhesives. J Adhesion 26;1988:273–91.

[12] Xu XX, Crocombe AD, Smith PA. Fatigue behaviour of joints bonded with either filled, or filled and toughened, adhesive. Int J Fatigue 1994;16:469–77.

[13] Dessureault M, Spelt JK. Observations of fatigue crack initiation and propagation in an epoxy adhesive. Int J Adhesion Adhesives 1997;17:183–95.

[14] Mall S, Ramamurthy G, Rezaizdeh MA. Stress ratio effect on cyclic debonding in adhesively bonded composite joints. Compos Struct 1987;8:31–45.

[15] Knox EM, Tan KTT, Cowling MJ, Hashim SA. The fatigue performance of adhesively bonded thick adherend steel joints. Proceedings of the European Adhesion Conference, vol. 1. Cambridge, UK, 1996. p. 319–24.

[16] Taylor D. Fatigue thresholds. London: Butterworths, 1989.

[17] Mangalgiri PD, Johnson WS, Everett RA. Effect of adherend thickness and mixed mode loading on debond growth in adhesively bonded composite joints. J Adhesion 1987;23:263–88.

[18] Jethwa JK. The fatigue performance of adhesively bonded metal joints. Ph.D. thesis, Imperial College, London, 1995.

[19] Mall S, Yun KT, Kochar NK. Characterization of matrix toughness effect on cyclic delamination growth in graphite fiber composites, ASTM STP 1012. Philadelphia: American Society for Testing and Materials, 1989. p. 296–310.

[20] Gustafson CG, Hojo M. Delamination fatigue crack growth in unidirectional graphite/epoxy laminates. J Reinforced Plast Compos 1987;6:36–52.

[21] Ewalds HL. Fracture mechanics. London, UK: Edward Arnold, 1984.

[22] Mall S, Yun KT. Effect of adhesive ductility on cyclic debond mechanism in composite-to-composite bonded joints. J Adhesion 1987;23:215–31.

[23] Xu XX, Crocombe AD, Smith PA. Fatigue crack growth rates in adhesive joints at different frequencies. J Adhesion 1996;58: 191–204.

[24] Mall S, Johnson WS. Characterization of mode I and mixed mode failure of adhesive bonds between composite adherends, ASTM STP 893. Philadelphia: American Society for Testing and Materials, 1986. p. 322–34.

[25] Jethwa JK, Kinloch AJ, Wallington G. A new test method for determining the adhesive fracture energy when bonding thin or coated substrates. J Mater Sci Lett 1995;14:155–7.

[26] Mostovoy S, Ripling EJ. Flaw tolerance of a number of commercial and experimental adhesives. Adhesion Sci Technol 1975;9B:513–562s.

[27] Kinloch AJ, Osiyemi S. Predicting the fatigue life of adhesively bonded joints. J Adhesion 1993;43:79–90.

[28] Curley AJ, Jethwa JK, Kinloch AJ, Taylor AC. The fatigue and durability behaviour of automotive adhesives. Part III: predicting the service life. J Adhesion 1998;66:39–59.

[29] Little MSG. The durability of structural adhesive joints. Ph.D. thesis, Imperial College, London, 1999.

[30] Pankevicius ER, Spicer M. Technique and apparatus for automatic monitoring of crack propagation along glue lines. J Mater Sci 1990;25:3079–82.

[31] Liaw PK, Logsdon WA, Roth LD, Hartmann HR. Krak-gages for automated fatigue crack growth rate testing: a review, ASTM STP 877. Philadelphia: American Society for Materials and Testing, 1985. p. 177–96.

[32] Liaw PK, Hartmann HR, Helm EJ. Corrosion fatigue crack propagation testing with the krak-gage in salt water. Eng Fract Mech 1983;1:121–1131.

[33] Griffith AA. Phil Trans Roy Soc 1920;A221:163.

[34] Davies P. Protocols for interlaminar fracture testing of composites. European Structural Integrity Society: Polymers and Composites Task Group, 1992.

[35] Hashemi S, Kinloch AJ, Williams JG. Corrections needed in double-cantilever beam tests for assessing the interlaminar failure of fibre-composites. J Mater Sci Lett 1989;8:125.

[36] Mostovoy S, Crosley PB, Ripling EJ. Use of crack-line-loaded specimens for measuring plane strain fracture toughness. J Mater 1967;2:661–81.

[37] Penado FE. A closed form solution for the energy release rate of the double cantilever beam specimen with an adhesive layer. J Compos Mater 1993;27:383–407.

[38] Olsson R. A simplified improved beam analysis of the DCB specimen. Compos Sci Technol 1992;43:329–38.

[39] Williams JG. Large displacement and end block effects in the 'DCB' interlaminar test in modes I and II. J Compos Mater 1987;21:331–47.

[40] Singh S, Greenhalgh E. Mixed –mode delamination growth in carbon-fibre composites under fatigue loading. DRA Technical Report DRA/SMC/CR961052/1.0, 1996.

[41] Kinloch AJ, Young RJ. Fracture behaviour of polymers. Barking, UK: Applied Science Publishers, 1983.

[42] Williams JG. Fracture mechanics of polymers. Chichester, UK: Ellis Horwood, 1984.

[43] Yee AF, Pearson RA. J Mater Sci 1986;21:2462.

[44] Garg AC, Mai YW. Failure mechanisms in toughened epoxy resins — a review. Compos Sci Technol 1988;31:179–223.

[45] Oba T. The fatigue behaviour of toughened epoxy polymers. Ph.D. thesis, Imperial College, London, 1999.

[46] Ashcroft IA, Abdel-Wahab MM, Crocombe AD, Hughes DJ, Shaw SJ. The effect of environment on the fatigue of bonded composite joints. Part 1: testing and fractography. Composites: Part A 2001;32:45–58.

[47] Brussat TR, Chiu ST. Fracture mechanics for structural adhesive bonds—final report. AFML TR-77-163, Air Force Materials Laboratory, 1977.

[48] Papini M, Fernlund G, Spelt JK. The effect of geometry on the fracture of adhesive joints. Int J Adhesion Adhesives 1994;14:5–13.

[49] Johnson WS. Stress analysis of the cracked-lap-shear specimen: an ASTM round robin. J Test Eval 1987;15:303–24.

[50] Mall S, Johnson WS. Characterization of mode I and mixed-mode failure of adhesive bonds between composite adherends. NASA-TM-86355, National Aeronautics and Space Administration, 1985.
[51] Abdel-Wahab MM, Ashcroft IA, Crocombe AD, Hughes DJ, Shaw SJ. The effect of environment on the fatigue of bonded composite joints. Part 2: fatigue threshold prediction. Composites: Part A 2001;32:59–69.
[52] Abdel-Wahab MM, Ashcroft IA, Crocombe AD, Shaw SJ. Prediction of fatigue thresholds in adhesively bonded joints using damage mechanics and fracture mechanics. J Adhesion Sci Technol 2001;15:763–82.
[53] Pradhan SC, Iyengar NGR, Kishore NN. Finite element analysis of crack growth in adhesively bonded joints. Int J Adhesion Adhesives 1995;15:33–41.